BioOne COMPLETE

Monte Carlo Simulation of SARS-CoV-2 Radiation-Induced Inactivation for Vaccine Development

Authors: Francis, Ziad, Incerti, Sebastien, Zein, Sara A., Lampe, Nathanael, Guzman, Carlos A., et al.

Source: Radiation Research, 195(3) : 221-229

Published By: Radiation Research Society

URL: https://doi.org/10.1667/RADE-20-00241.1

BioOne Complete (complete.BioOne.org) is a full-text database of 200 subscribed and open-access titles in the biological, ecological, and environmental sciences published by nonprofit societies, associations, museums, institutions, and presses.

Your use of this PDF, the BioOne Complete website, and all posted and associated content indicates your acceptance of BioOne's Terms of Use, available at www.bioone.org/terms-of-use.

Usage of BioOne Complete content is strictly limited to personal, educational, and non - commercial use. Commercial inquiries or rights and permissions requests should be directed to the individual publisher as copyright holder.

BioOne sees sustainable scholarly publishing as an inherently collaborative enterprise connecting authors, nonprofit publishers, academic institutions, research libraries, and research funders in the common goal of maximizing access to critical research.

Downloaded From: https://bioone.org/journals/Radiation-Research on 28 Mar 2024
Terms of Use: https://bioone.org/terms-of-use

RADIATION RESEARCH **195**, 221–229 (2021)
0033-7587/21 $15.00
©2021 by Radiation Research Society.
All rights of reproduction in any form reserved.
DOI: 10.1667/RADE-20-00241.1

Monte Carlo Simulation of SARS-CoV-2 Radiation-Induced Inactivation for Vaccine Development

Ziad Francis,[a] Sebastien Incerti,[b] Sara A. Zein,[b] Nathanael Lampe,[b,1] Carlos A. Guzman[c] and Marco Durante[d,e,2]

[a] *Saint Joseph University, U.R. Mathématiques et Modélisation, Beirut, Lebanon;* [b] *Université de Bordeaux, CNRS/IN2P3, UMR5797, Centre d'Études Nucléaires de Bordeaux Gradignan, France;* [c] *Helmholtz Zentrum für Infektionsforschung (HZI), Department of Vaccinology and Applied Microbiology, Braunschweig, Germany;* [d] *GSI Helmholtzzentrum für Schwerionenforschung, Biophysics Department, Darmstadt, Germany; and* [e] *Technische Universität Darmstadt, Institute of Condensed Matter Physics, Darmstadt, Germany*

Francis, Z., Incerti, S., Zein, S. A., Lampe, N., Guzman, C. A. and Durante, M. Monte Carlo Simulation of SARS-CoV-2 Radiation-Induced Inactivation for Vaccine Development. *Radiat. Res*. 195, 221–229 (2021).

Immunization with an inactivated virus is one of the strategies currently being tested towards developing a SARS-CoV-2 vaccine. One of the methods used to inactivate viruses is exposure to high doses of ionizing radiation to damage their nucleic acids. While gamma (γ) rays effectively induce lesions in the RNA, envelope proteins are also highly damaged in the process. This in turn may alter their antigenic properties, affecting their capacity to induce an adaptive immune response able to confer effective protection. Here, we modeled the effect of sparsely and densely ionizing radiation on SARS-CoV-2 using the Monte Carlo toolkit Geant4-DNA. With a realistic 3D target virus model, we calculated the expected number of lesions in the spike and membrane proteins, as well as in the viral RNA. Our findings showed that γ rays produced significant spike protein damage, but densely ionizing charged particles induced less membrane damage for the same level of RNA lesions, because a single ion traversal through the nuclear envelope was sufficient to inactivate the virus. We propose that accelerated charged particles produce inactivated viruses with little structural damage to envelope proteins, thereby representing a new and effective tool for developing vaccines against SARS-CoV-2 and other enveloped viruses. **© 2021 by Radiation Research Society**

INTRODUCTION

The threat from the new SARS-CoV-2 is omnipresent in all regions of the world (*1*). Several companies and research groups are reporting promising results in the development of vaccines (*2–4*). Some of the SARS-CoV vaccines developed to date follow the traditional approach based on inactivated or live attenuated viruses (*5–8*). The SARS-CoV-2 virus is sensitive to the standard inactivation methods used for producing vaccines against other viral diseases (*9*). However, traditional chemical inactivation methods can lead to the modification of critical epitopes in both inactivated and subunit vaccines, thereby affecting overall vaccine efficacy (*10*). Although live attenuated virus-based vaccines generally induce potent cellular immune response, antibody production is often less efficient, and the use of attenuated viruses is often not indicated in individuals who are immunosuppressed as a result of disease or therapeutic interventions. In the current pandemics, mRNA vaccines are emerging as very attractive alternatives, due to their ease of manufacture and potent immune response (*11*), but their long-term effectiveness and safety remains to be elucidated in comparison to the well-established inactivated virus standard.

Among inactivation methods, radiation technology remains of interest to vaccine manufacturers, because it penetrates pathogens to damage the nucleic acid without residual chemical contaminants (*12, 13*). Nevertheless, the development of irradiated vaccines has not been pursued actively over the past 20 years for two main reasons: 1. The development of new radiation techniques has been considered impractical or difficult due to issues accessing radiation equipment (*14*); and 2. It has been thought that modern subunit vaccines would provide a solution, since they can be developed more easily (*15*). However, recent successful development of irradiated vaccines for human malaria (*16*) and influenza (*17, 18*) have not only demonstrated the feasibility and practicality of this technique, but also the efficacy of such vaccination approaches, prompting research in applying the method to other viruses (*19, 20*). Yet, it is known that high-dose γ-ray exposure can damage epitopes necessary to elicit the immune response (*21*). Formaldehyde and other chemicals commonly used for virus inactivation also induce severe damage to the protein structures involved in the elicitation of adaptive immune response after vaccination (*22*).

With conventional γ-ray sterilization, many photons are needed to induce lesions in RNA. However, the track

[1] This author now works for a private company.

[2] Address for correspondence: GSI, Planckstrasse 1, Darmstadt, Hessen 64291, Germany; email: m.durante@gsi.de.

Downloaded From: https://bioone.org/journals/Radiation-Research on 28 Mar 2024
Terms of Use: https://bioone.org/terms-of-use

structure of charged particles, such as those used in cancer therapy (*23*), suggests that a single traversal is sufficient to induce lethal lesions in RNA with minimal membrane damage (*13*). In this work we performed a comprehensive simulation of ionizing radiation damage to the SARS-CoV-2 using Geant4-DNA (*24*), a Monte Carlo simulation toolkit which is used for modeling biological damage induced by ionizing radiation at the DNA scale. We developed a Geant4-DNA application to simulate the SARS-CoV-2 structure and calculated the damage to the virus's spike and membrane proteins, and the viral RNA after exposure to radiations of different quality, i.e., low- or high-linear-energy-transfer (LET) radiation. High-LET radiation is densely ionizing and may inactivate the virus with less membrane damage than low-LET (sparsely ionizing) radiation.

MATERIALS AND METHODS

Physics Processes and Radiation Particles

The incident radiation used was a parallel beam with a circular cross section 132 nm in diameter, uniformly covering the complete geometry of the virus including the spike proteins. Simulations were performed for 3-MeV alpha (α) particles, 450-MeV/amu ^{56}Fe ions, 80-MeV/amu ^{12}C ions, 2-keV and 200-keV electrons, 80-MeV and 30-MeV protons and a ^{60}Co γ-ray spectrum (1.17 and 1.32 MeV).

The Geant4-DNA processes (*25–28*) were used to simulate step-by-step tracks of ions and electrons. The Livermore models (*29, 30*) were used to simulate gamma interactions. Processes included for protons and α particles were nuclear scattering, electronic excitation, ionization and charge transfer. For electrons, elastic scattering, electronic excitation, ionization, vibrational and rotational excitations, and electron attachment were considered. Electrons were followed down to 7.5 eV; below this energy an electron goes one additional solvation step and its remaining energy is locally deposited. Heavy ion interactions consisted only of ionization, which was simulated using the relativistic Rudd model with an effective charge scaling as described elsewhere (*31*) and previously used for carbon ion fragments (*32*).

Since all the included processes of Geant4-DNA were validated for liquid water, we proceeded with a density scaling to account for the different virus materials. Therefore, the different protein densities were calculated based on the constitution mentioned in (*33*) and the cross sections were scaled accordingly. The calculated densities are 1.4 g/cm^3 for the spike proteins, 1.38 g/cm^3 for the membrane protein and 1.46 g/cm^3 for the inner sphere, equal to the RNA density.

Simulation of Radiation-Induced Damage

Energy deposition points were calculated in the spike proteins, membrane proteins and RNA molecule. The RNA size was calculated based on the genome sequence published by the National Center for Biotechnology Information (*34*). The viral ss-RNA sequence length is 29,903 bases and its mass is ~9,584 MDa. Considering the RNA density, we can estimate its approximate volume to be ~10,900 nm^3. This value is equal to ~4% of the inner volume of the virus, the 80-nm sphere shown in Fig. 1. Therefore, for each energy deposition point inside the virus a random sampling was applied with a 4% probability that this point is positioned on the RNA. In a recently published study (*35*) using the Monte Carlo code TOPAS, investigation was performed on different RNA setups with fast ion irradiation showing differences in the extreme case where RNA is densely centered in the middle of the capsid. The assumption that RNA is homogeneously distributed inside the virus was previously used elsewhere (*36*) for DNA damage assessment after proton irradiations, leading to reasonable results. While modeling the RNA at the atomistic level is still the reference method, the approximation of a homogeneous geometrical cross section is simpler to incorporate in such comparative studies. In an earlier study (*36*) this method was validated for DNA irradiation where the obtained single- and double-strand-break ratios were in agreement with experiments and detailed atomistic calculations (*37*). Although this approach was never validated for viral RNA, due to lack of specific RNA irradiation data, we could consider that RNA geometry and positioning vary within a population of viral structures. Therefore, considering a large amount of virus targets, with different RNA distributions, irradiated by a uniform beam, the homogeneous RNA cross section is an average approximation. Moreover, other simulations were performed while changing the cross section relative value by 25%, meaning that considering 3% RNA volume instead of 4% does not affect our results by a visible amount, since our conclusions rely mainly on comparisons among different particle types.

Although the uniform RNA model presented here is suitable for numerical simulations, it does not provide a differentiation between sugar-phosphate and nitrogenous bases damage. Therefore, any RNA damage was considered sufficient to inactivate the virus.

Studies published in the literature on DNA damage reported breaks induced by low-energy electrons. The incident energies ranged between 1 eV and 30 eV (*38–41*), and damage was induced by energies as low as 3–5 eV. Taking these values into account we determined that an energy deposition above a threshold of 10 eV, positioned on the RNA volume, is considered a damage.

For spike proteins, if the sum of energy depositions inside one protein was higher than the 10-eV damage energy threshold, we consider the protein as damaged. The number of damaged proteins was counted and normalized to a single RNA damage. As we were looking for the ionizing radiation type that would yield the lowest amount of protein damage per RNA damage to inactivate the virus, this normalization is desirable. In a second stage, to verify the influence of the damage threshold on our results, calculations were evaluated for four different threshold values: 5, 10, 15 and 20 eV.

RESULTS

Simulation Setup

The Geant4-DNA extension (*24, 26–28*) of the Geant4 Monte-Carlo toolkit (*30, 42, 43*) was used to simulate ionizing particle tracks and energy deposition inside the virus model. The virus membrane was represented by a spherical volume, and the outer and inner diameters were set to 100 nm and 80 nm, respectively. These dimensions are based on experimental data from the literature. The virus size reported by published experiments varies between 60 nm and 140 nm (*44–47*), meaning an average of 100 nm is a reasonable estimation. A total of 166 membrane proteins were modeled, represented by cylindrical volumes 6 nm in diameter and 6 nm in height homogeneously distributed within the 10-nm-thick membrane. The spike proteins were modeled by conical volumes with base and top diameters of 6 nm and 14 nm, and 16 nm height. A total of 141 spike protein volumes were homogeneously distributed on the outside of the membrane. Figure 1 shows the configuration of the described virus structure. The approximate dimensions of the proteins of the SARS-CoV-2 were estimated based on the descriptions from the protein data bank (*48,*

Downloaded From: https://bioone.org/journals/Radiation-Research on 28 Mar 2024
Terms of Use: https://bioone.org/terms-of-use

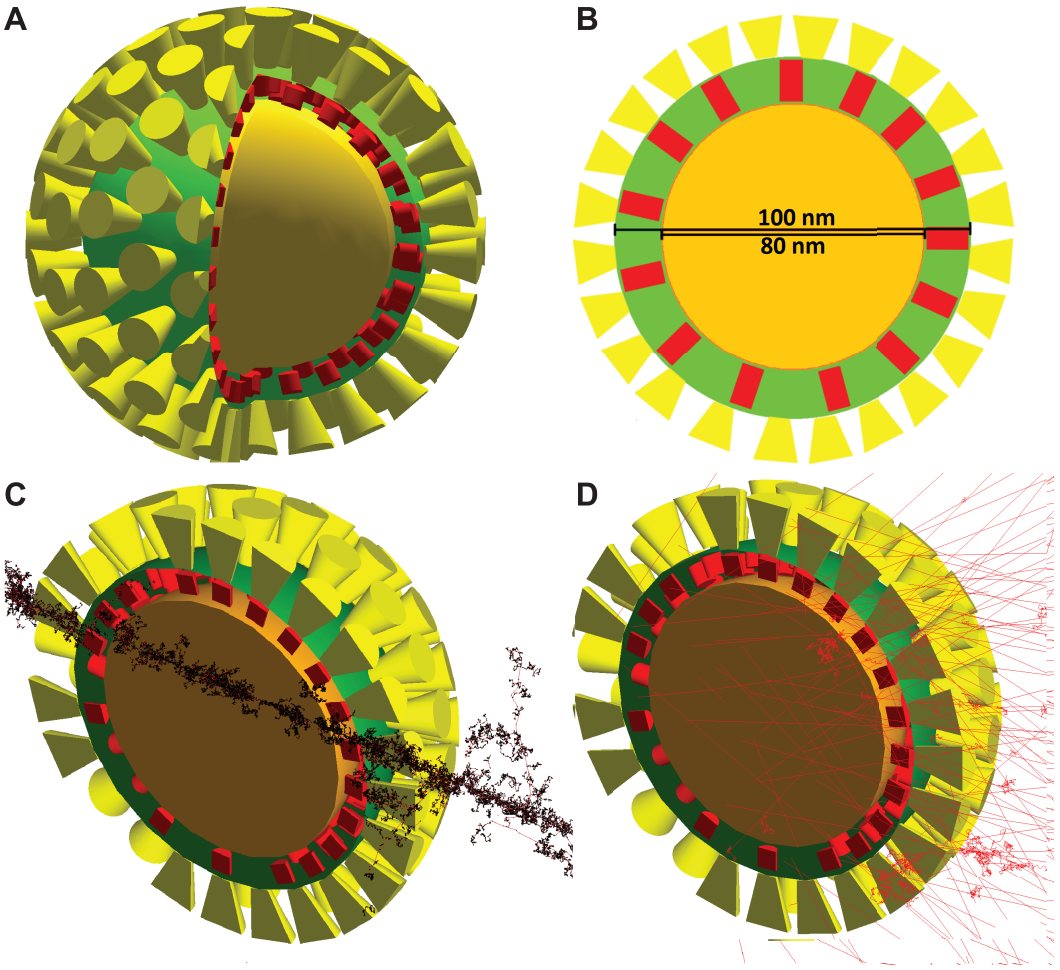


FIG. 1. Geometry of the virus model implemented in the simulation. Yellow cones represent the spike proteins, the membrane proteins, shown in red, are distributed within the membrane shown in green (panels A and B). The inner sphere represents the inside volume of the virus that usually holds the RNA. A 450-MeV/amu iron ion track is also shown crossing the virus volume with secondary electrons tracks (panel C) and cobalt γ electrons are shown in (panel D).

49). The nucleic acid contained in the envelope is a ss-RNA of approximately 30 kbp (*1*).

Damage Distribution

For a comparison of sparsely and densely ionizing radiation in the SARS-CoV-2 target, Fig. 2 shows the simulation of the damage produced in the virus by: ^{60}Co γ rays (LET = 0.24 keV/μm), the standard radiation used for virus inactivation in vaccine development; 3-MeV α particles, a common standard in high-LET radiation (LET = 126 keV/μm) with a range of only 18 μm in water; and ^{56}Fe 450 MeV/amu (LET = 178 keV/μm), a densely ionizing ion often used at accelerators in studies of space radiation protection (*50*) and with a range of approximately 12 cm in water. Probability distributions of the number of RNA damage sites were normalized per 1 eV of energy deposition.

The first bin of the distribution, showing the probability that no damage is induced, is highest for γ electrons. This bin constitutes ~90% of the total damage probability, meaning that the probability of inducing at least one RNA damage is only 10%. For Fe ions the damage probability is almost 77% of the whole spectrum, and it becomes 99.8% if only ion traversals though the nuclear envelope are considered.

The number of RNA lesions per incident particle reaches up to ~40 damage points for Fe ions with a probability of 10^{-7} per eV, while the largest number observed for γ electrons is ~9 with a probability of 10^{-7} per eV. Since these numbers are of very low probability and for the sake of clarity, the figure visible range was limited to 30 damage points showing the main differences between ions and γ electron damage spectra.

Figure 2 (right-side column) also shows the distribution of the number of damaged spike proteins for particles and γ electrons, normalized per 1 eV of energy deposition, showing a higher damage yield for densely ionizing charged particles. Ideally, we would be looking for a radiation type

Downloaded From: https://bioone.org/journals/Radiation-Research on 28 Mar 2024
Terms of Use: https://bioone.org/terms-of-use

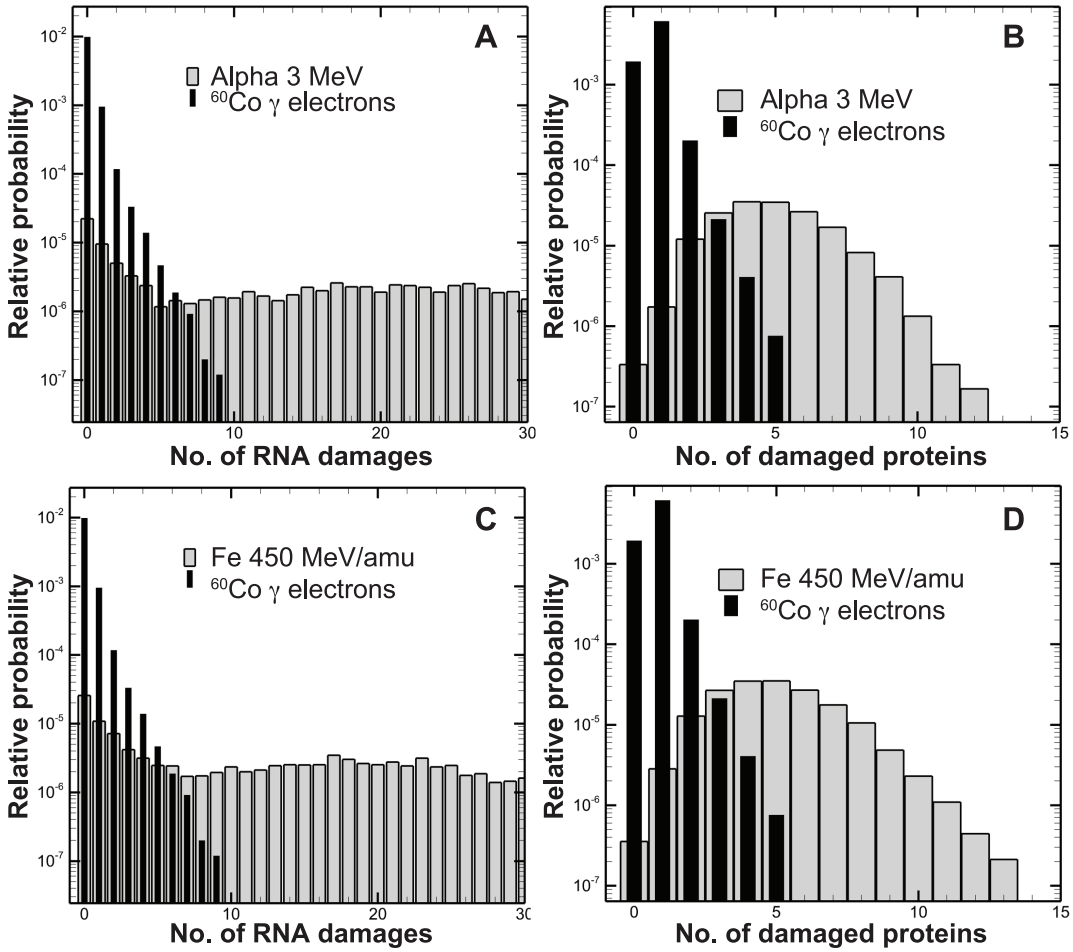


FIG. 2. Distributions of the number of RNA damage events, and the number of damaged spike proteins. Results are shown for α particles and ^{60}Co γ electrons (panels A and B), Fe ions and Co γ electrons (panels C and D). Results are normalized per energy deposition of 1 eV.

leading to a high RNA damage yield and a small number of damaged proteins.

However, the apparently higher number of damaged proteins is simply due to the dense ionizing track that has a high probability to damage any protein when traversing it. In Fig. 2 we focus on the damage in the nucleic acid (single-stranded RNA) and the spike proteins, which is considered the main antigen target for the SARS-CoV-2 vaccine.

Ratio of Protein/RNA Damage

The average number of damaged spike proteins normalized to a single RNA break is shown in Fig. 3 for different incident particles according to their LET. In addition to the particles shown in Fig. 2, we have included the following: protons at 30 MeV and 80 MeV, accelerated at cyclotrons for radionuclide production or eye tumor therapy; ^{12}C ions at 80 MeV/amu, available in several research and medical accelerators (*51*); and electrons, which are used for sterilization of surfaces (*52*). The electron energy of 200 keV was selected since that electron beam was studied experimentally as an alternative to γ rays for vaccine production (*53*). A second electron energy of 2 keV was also selected based on the results of the recent Monte Carlo study by Feng *et al*. (*33*) which show that at this energy there is a maximum efficiency in virus sterilization by electrons. We found a decreasing damage ratio with increasing LET, and the minimum value, ~0.4, is obtained using α particles and iron ions. The ratio for γ rays and 200-keV e^- is ~6–7. The high ratio obtained for conventional γ rays is due to a low average value of the RNA damage distribution.

The estimated survival curves were calculated considering that one RNA single-strand break is sufficient to inactivate the virus, as it cannot be repaired and will result in an interrupted amino acid chain. Thus, the probability of inducing at least one RNA damage was used in the exponential survival model:

$$S = e^{-\sigma F},$$

where σ is the cross section for RNA single-strand break induction in the virus (calculated using Monte Carlo simulation) and F is the incident particle fluence. Expo-

Downloaded From: https://bioone.org/journals/Radiation-Research on 28 Mar 2024
Terms of Use: https://bioone.org/terms-of-use

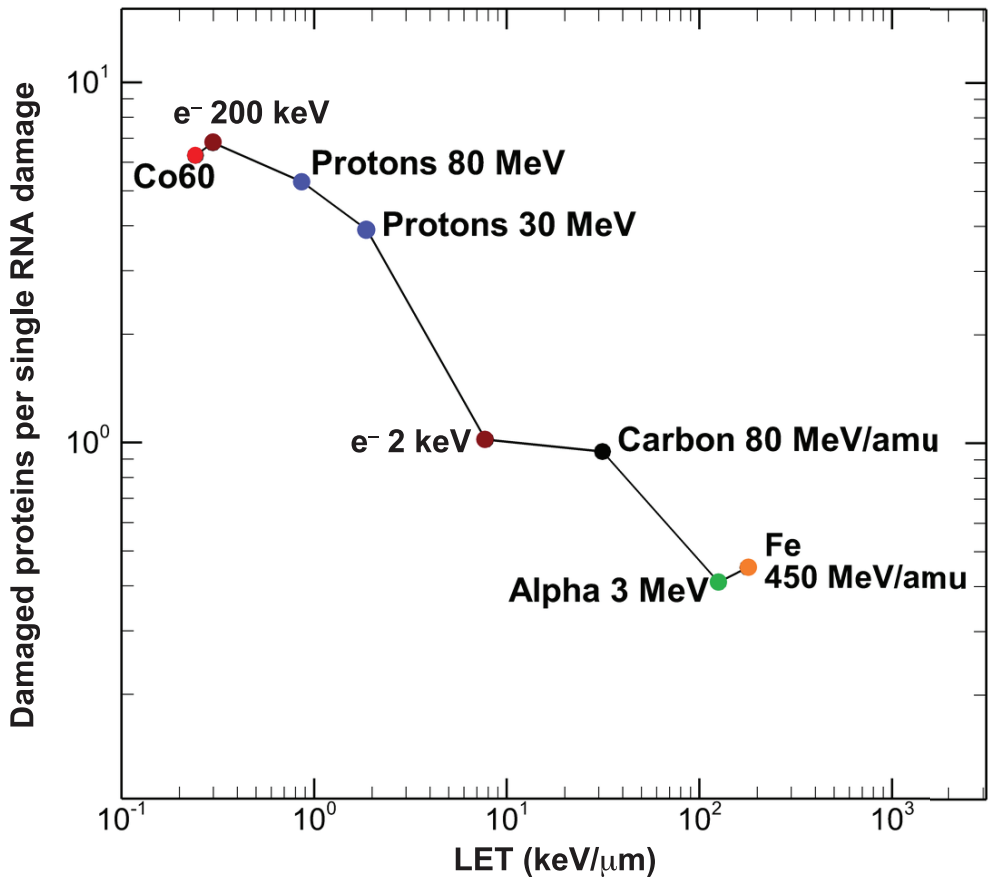


FIG. 3. Relative amount of membrane protein damage per RNA lesion. The number of damaged spike proteins per single RNA break is plotted versus particle LET. Low membrane/RNA damage ratios are associated with a better viral product for vaccine development, while high values indicate that the inactivated virus also has severe damage in the epitopes.

nential survival curves are essentially always found in irradiation of viruses or proteins, lacking repair capability (*13*).

Figure 4 shows the SARS-CoV-2 survival probability as a function of the dose for sparsely and densely ionizing particles. As expected, high-LET irradiation requires a much higher dose to inactivate the virus because the dose is proportional to the LET and the particle fluence must remain high enough to hit all the targets.

Robustness of the Simulation

As explained in the Materials and Methods section, calculations presented in Figs. 2, 3 and 4 were obtained using a 10-eV threshold of the biological molecule damage. Even if this number is sound, variations in the range of 5–20 eV have been used in the literature (*37, 54, 55*), and it is therefore necessary to assess the robustness of our simulation to this parameter. Figure 5 shows the average number of damaged spike (Fig. 5A) and membrane (Fig. 5C) proteins normalized by a single RNA break versus the energy damage threshold using values of 5 eV, 10 eV, 15 eV and 20 eV. The ratio increases with increasing damage threshold for all radiation qualities. In fact, increasing the threshold discards all the ionization points below a certain value. Considering that each RNA ionization is a damage event in the absence of repair mechanisms (as occurs in mammalian cells), increasing the threshold simply decreases the overall number of RNA damage events. Accounting for the lowest ionization binding energy in Geant4-DNA being 10.73 eV, it is in fact expected that damage ratios increase as the threshold value rises above 10 eV.

The robustness analysis should consider whether the LET dependence of the ratio (Fig. 5) is affected by the modified protein/RNA ratio. Figure 5B and D shows the ratio of the results obtained for the different particles in the left-side panel, for spike and membrane proteins, respectively, formalized to the reference radiation source (γ rays). Results for 5-eV and 10-eV thresholds are almost similar, since ionization is triggered at 10.73 eV but above this value the increase in the damage ratio becomes more significant. Notably, the ordering of the different particles is not influenced by the threshold except for electrons versus carbon ions above a threshold of 15 eV, which is seen in both parts related to spike proteins in Fig. 5A and B.

Downloaded From: https://bioone.org/journals/Radiation-Research on 28 Mar 2024
Terms of Use: https://bioone.org/terms-of-use

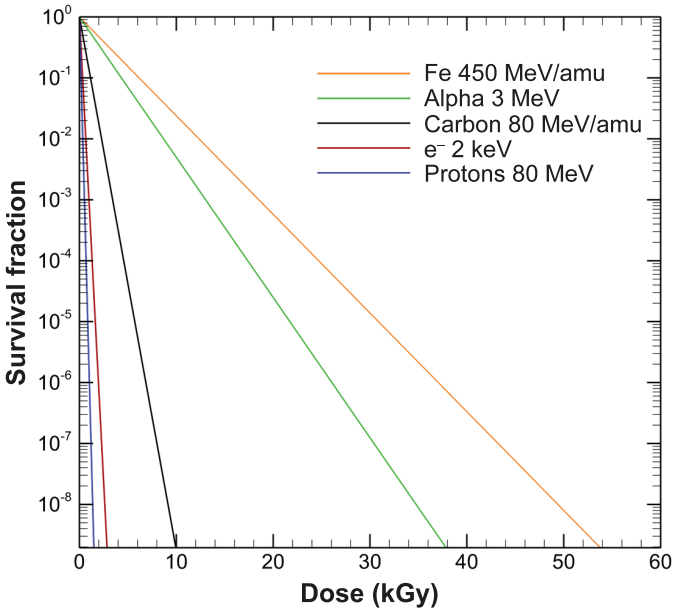


FIG. 4. Estimated survival curves of SRAS-CoV-2 for different particle types.

DISCUSSION

Simulation of radiation damage in SARS-CoV-2 is interesting for many reasons. Here, we analyze the potential use of ionizing radiation for virus inactivation in vaccine manufacturing. As with other chemical agents, conventional inactivation using γ rays unavoidably damages the membrane proteins, whereas ideally an inactivated virus with intact membrane antigens would elicit the most effective vaccine response. Here, we show that when densely ionizing charged particles such as accelerated heavy ions or α particles are used, the ratio of protein/RNA damage is reduced by more than an order of magnitude (Fig. 3).

Charged particles can, therefore, represent a powerful tool for developing SARS-CoV-2 and other vaccines based on inactivated virus, which is still one of the strategies currently used for pandemics.

While Geant4-DNA is validated as an accurate Monte Carlo code for microscopic calculations, every model is affected by uncertainty, and in particular the minimum energy required to induce damage. While the minimum energy for damage in nucleic acids, characterized by strand

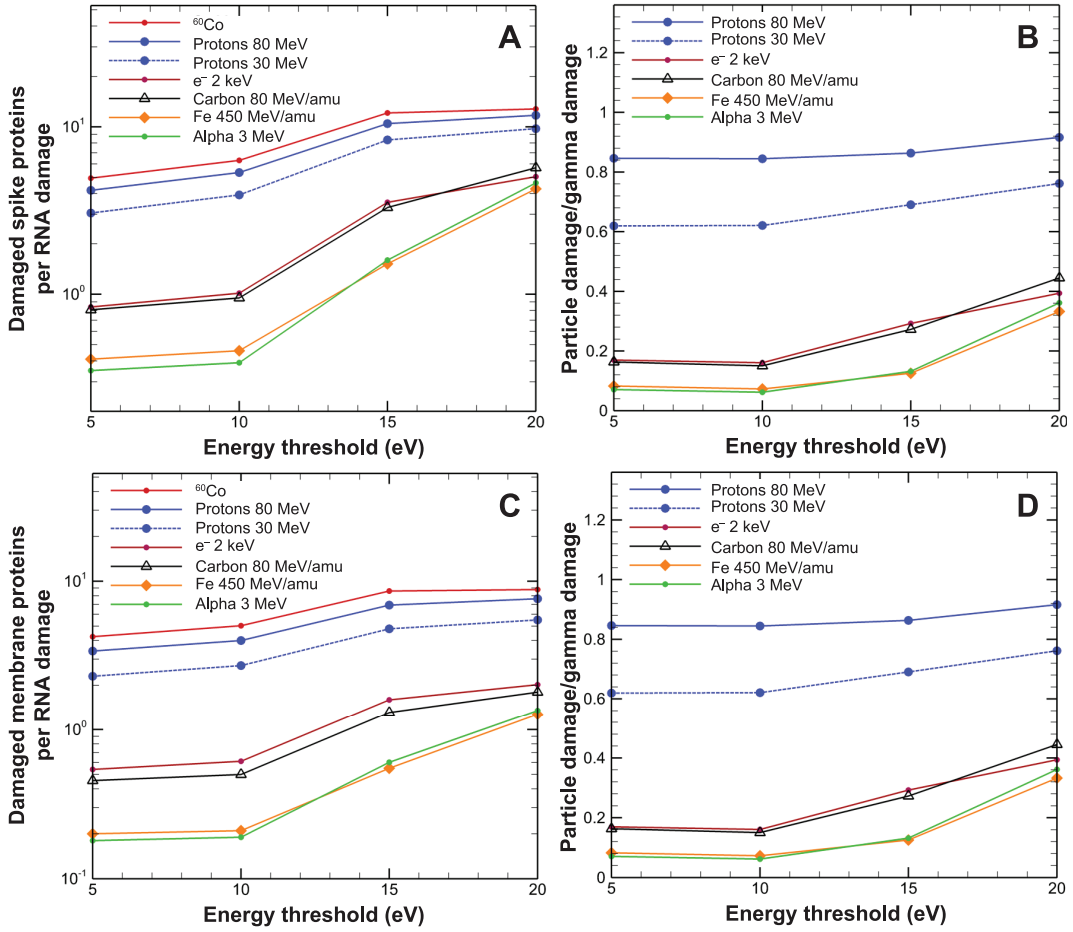


FIG. 5. Protein and membrane damage comparison for different radiation types. Number of spike (panel A) and membrane (panel C) protein damage per RNA break were calculated for different damage energy thresholds and for different incident particle types. Ratios of protein damage for the different particles to protein damage obtained with gamma rays are also shown for spike proteins (panel B) and membrane proteins (panel D).

Downloaded From: https://bioone.org/journals/Radiation-Research on 28 Mar 2024
Terms of Use: https://bioone.org/terms-of-use

breaks, is well known, this uncertainty is even higher for proteins, where the energy required for a conformational change, leading to a failed recognition as an antigen, could be higher. However, we have shown that our conclusions are robust in relationship to the threshold energy for damage (Fig. 5), meaning the advantage of densely ionizing radiation remains, or could even be bigger by an order of magnitude, with different simulation parameters.

In this study we only considered direct radiation effects on proteins and RNA, disregarding the indirect effects from free radicals. This is acceptable for high-LET radiation since most of the damage comes from direct effects. However, for low-LET radiation, indirect effects are an important part of the total result, especially for RNA. Moreover, the free radical damage to proteins is still unclear and related models are not available to be included in such numerical studies. Therefore, results obtained for low-LET radiation might underestimate the RNA damage by a certain percentage. This would probably further enhance the advantages of densely ionizing radiation, but while it is possible to simulate the complete RNA geometry and the chemical species diffusion using Geant4-DNA, the interactions of free radicals with specific proteins and their effects on the role of spike proteins is as yet unknown. Moreover, the virus inactivation for vaccine production generally occurs in dry ice, and this highly reduces the influence of the indirect effects.

Since an average size of 100-nm diameter was considered for our virus geometry, we expect that our results stand for the average effect of radiation on viruses with 60- to 140-nm diameter sizes as presented in this work. In fact, for large dimensions we expect an increased spacing among membrane proteins and RNA molecules, resulting in slightly lower energy deposition rates for both targets. However, the difference is not expected to affect the ratio between proteins and RNA damages since both will have lower values. In the opposite case for smaller reported dimensions, the separation between molecules will decrease, and therefore we expect a slightly higher radiation effect due to the higher molecular density, so the ratio is not expected to be drastically affected since both the membrane proteins and the RNA damage rates will increase.

While the simulations clearly suggest that accelerated heavy ions can be a powerful tool for vaccine development, the practical implementation is very difficult. Energetic charged particles require large accelerators and high doses. As shown in Fig. 4, inactivation doses for heavy ions are higher than for γ rays. Survival curves similar to those in Fig. 4 have been measured previously for many different viruses (*56–58*). The increase in lethal dose is simply due to the fact that $D(Gy) = LET \times$ fluence, and the fluence (in particles per cm^2) must be very high to hit all the viruses in the target samples, according to Poisson statistics.

The best particle for virus inactivation with minimal membrane damage depends on the LET (Fig. 3) and also on the track structure, similar to biological effects in mammalian cells (*59*). However, the choice of the best ion will be dominated by practical considerations. Large numbers of viruses must be irradiated in closed cryovials in dry ice to keep the virus frozen (*60*). Particles with very small penetration range (such as α particles and low-energy electrons) are unable to penetrate the wall of a cryovial. Concerning electrons, our results support the experimental data showing that inactivation with a 200-keV electron beam maintains the antigenic properties of γ rays (*53*), and that in principle, slow (2-keV) electrons would be more efficient (*33*), but the short range of these electrons (in water, $\sim$0.45 mm at 200 keV and $\sim$0.2 μm at 2 keV) hampers their practical usage.

High-energy heavy ions, such as the Fe ions simulated in this work, are more suitable for vaccine production because they are both high LET and long range, so whole cryoboxes can be irradiated in one session. High beam intensity is required to reach a kGy-level dose in a short time. In a preliminary safety test at the SIS18 synchrotron at GSI (Darmstadt, Germany), a high-intensity and -energy synchrotron (*61*), we found that a few kGy of 1 GeV/n Fe ions ($\sim$28 cm range in water) can be delivered to cryoboxes containing many frozen cryovials surrounded by dry ice in a few hours, without any damage to the container and with limited and quickly reduced sample activation. These tests show that such irradiations are feasible and can represent a completely new application of large-scale particle accelerators currently in operation and under construction worldwide (*62*).

In conclusion, our Monte Carlo simulations show that inactivation of SARS-CoV-2 can be achieved with accelerated heavy ions minimizing the damage to the epitopes in membrane proteins. Validation experiments at accelerators will be necessary to compare the capacity to induce antibody- and cell-mediated immune responses of viruses inactivated by either heavy ions or conventional methods.

While it would currently be impossible to have mass production in large heavy ion accelerators, cheaper technologies might be an alternative solution to produce high-LET radiation beams, e.g., commercial cyclotrons working at high intensity, or even high-activity α-particle sources. To reach irradiation of large amounts of viral particles, it is possible to use disposable bags and continuous flow of viruses in a thin film, a method developed for virus inactivation using 200-keV electrons, which demonstrated an ability to effectively inactivate influenza and other viruses in a reasonably short time (*63*). If the calculation performed in the current work is supported by experimental data, we expect that great effort will be undertaken to develop simple methods for collecting large quantities of high-LET radiation-inactivated viruses.

Downloaded From: https://bioone.org/journals/Radiation-Research on 28 Mar 2024
Terms of Use: https://bioone.org/terms-of-use

ACKNOWLEDGMENTS

The safety tests on high-dose irradiation of cryovials were performed in Cave A in the frame of FAIR Phase-0 supported by the GSI Helmholtzzentrum für Schwerionenforschung in Darmstadt (Germany). We thank Dr. Uli Weber and his crew for support in those tests. We thank IN2P3/CNRS for the support to SZ and Geant4-DNA. We also thank Prof. Dr. Frederick Currell for the valuable discussions and corrections on our first draft of this manuscript. ZF would like to thank Pr. Richard Maroun for the discussions.

Received: October 29, 2020; accepted: December 16, 2020; published online: January 7, 2021

REFERENCES

1. Wu F, Zhao S, Yu B, Chen Y-M, Wang W, Song Z-G, et al. A new coronavirus associated with human respiratory disease in China. Nature 2020; 579:265–9.
2. Amanat F, Krammer F. SARS-CoV-2 Vaccines: Status report. Immunity 2020; 52:583–9.
3. Voysey M, Clemens SAC, Madhi SA, Weckx LY, Folegatti PM, Aley PK, et al. Safety and efficacy of the ChAdOx1 nCoV-19 vaccine (AZD1222) against SARS-CoV-2: an interim analysis of four randomised controlled trials in Brazil, South Africa, and the UK. Lancet 2020; Epub ahead of print.
4. Polack FP, Thomas SJ, Kitchin N, Absalon J, Gurtman A, Lockhart S, et al. Safety and efficacy of the BNT162b2 mRNA Covid-19 vaccine. N Engl J Med 2020; 383:2603–15.
5. Gao Q, Bao L, Mao H, Wang L, Xu K, Yang M, et al. Development of an inactivated vaccine candidate for SARS-CoV-2. Science 2020; 369:77–81.
6. Wang H, Zhang Y, Huang B, Deng W, Quan Y, Wang W, et al. Development of an inactivated vaccine candidate, BBIBP-CorV, with potent protection against SARS-CoV-2. Cell 2020; 182:713–21.e9.
7. Xia S, Zhang Y, Wang Y, Wang H, Yang Y, Gao GF, et al. Safety and immunogenicity of an inactivated SARS-CoV-2 vaccine, BBIBP-CorV: a randomised, double-blind, placebo-controlled, phase 1/2 trial. Lancet Infect Dis 2020; 21:39–51.
8. Xia S, Duan K, Zhang Y, Zhao D, Zhang H, Xie Z, et al. Effect of an inactivated vaccine against SARS-CoV-2 on safety and immunogenicity outcomes. JAMA 2020; 324:951–60.
9. Scheller C, Krebs F, Minkner R, Astner I, Gil-Moles M, Wätzig H. Physicochemical properties of SARS-CoV-2 for drug targeting, virus inactivation and attenuation, vaccine formulation and quality control. Electrophoresis 2020; 41:1137–51.
10. Pitisuttithum P, Chokephaibulkit K, Sirivichayakul C, Sricharoenchai S, Dhitavat J, Pitisuthitham A, et al. Antibody persistence after vaccination of adolescents with monovalent and combined acellular pertussis vaccines containing genetically inactivated pertussis toxin: a phase 2/3 randomised, controlled, non-inferiority trial. Lancet Infect Dis 2018; 18:1260–8.
11. Sahin U, Muik A, Derhovanessian E, Vogler I, Kranz LM, Vormehr M, et al. COVID-19 vaccine BNT162b1 elicits human antibody and TH1 T cell responses. Nature 2020; 586:594–9.
12. Pollard E. Inactivation of viruses for vaccine purposes using ionizing radiation and heat. Yale J Biol Med 1957; 29:436–43.
13. Durante M, Schulze K, Incerti S, Francis Z, Zein S, Guzman CA. Virus irradiation and COVID-19 disease. Front Phys 2020; 8.
14. Seo HS. Application of radiation technology in vaccines development. Clin Exp Vaccine Res 2015; 4:145–58.
15. Li L, Guo P, Zhang X, Yu Z, Zhang W, Sun H. SARS-CoV-2 vaccine candidates in rapid development. Hum Vaccin Immunother 2020; 1–10.
16. Arama C, Troye-Blomberg M. The path of malaria vaccine development: challenges and perspectives. J Intern Med 2014; 275:456–66.
17. Pica N, Palese P. Toward a universal influenza virus vaccine: Prospects and challenges. Annu Rev Med 2013; 64:189–202.
18. Chen F, Seong Seo H, Ji HJ, Yang E, Choi JA, Yang JS, et al. Characterization of humoral and cellular immune features of gamma-irradiated influenza vaccine. Hum Vaccin Immunother 2020; 1–12.
19. Shahrudin S, Chen C, David SC, Singleton E V., Davies J, Kirkwood CD, et al. Gamma-irradiated rotavirus: A possible whole virus inactivated vaccine. PLoS One 2018; 13:e0198182.
20. Marzi A, Halfmann P, Hill-Batorski L, Feldmann F, Shupert WL, Neumann G, et al. An ebola whole-virus vaccine is protective in nonhuman primates. Science 2015; 348:439–42.
21. Tobin GJ, Tobin JK, Gaidamakova EK, Wiggins TJ, Bushnell R V., Lee W-M, et al. A novel gamma radiation-inactivated sabin-based polio vaccine. PLoS One 2020; 15:e0228006.
22. Astill J, Alkie T, Yitbarek A, Taha-Abdelaziz K, Bavananthasivam J, Nagy E, et al. Examination of the effects of virus inactivation methods on the induction of antibody- and cell-mediated immune responses against whole inactivated H9N2 avian influenza virus vaccines in chickens. Vaccine 2018; 36:3908–16.
23. Durante M, Paganetti H. Nuclear physics in particle therapy: a review. Rep Prog Phys 2016; 79:096702.
24. Incerti S, Brown JMC, Guatelli S. Advances in Geant4 applications in medicine. Phys Med 2020; 70:224–7.
25. Incerti S, Ivanchenko A, Karamitros M, Mantero A, Moretto P, Tran HN, et al. Comparison of GEANT4 very low energy cross section models with experimental data in water. Med Phys 2010; 37:4692–708.
26. Bernal MA, Bordage MC, Brown JMC, Davídkova M, Delage E, El Bitar Z, et al. Track structure modeling in liquid water: A review of the Geant4-DNA very low energy extension of the Geant4 Monte Carlo simulation toolkit. Phys Med 2015; 31:861–74.
27. Incerti S, Kyriakou I, Bernal MA, Bordage MC, Francis Z, Guatelli S, et al. Geant4-DNA example applications for track structure simulations in liquid water: A report from the Geant4-DNA Project. Med Phys 2018; 45:e722–39.
28. Incerti S, Baldacchino G, Bernal M, Capra R, Champion C, Francis Z, et al. The GEANT4-DNA project. Int J Model Simulation Sci Comput 2010; 01:157–78.
29. Cullen D, Hubbell J, Kissel L. EPDL97: the evaluated photo data library '97 version. Oak Ridge, TN: U.S. Department of Energy/ Office of Scientific and Technical Information; 1997. (https://www.osti.gov/biblio/295438)
30. Allison J, Amako K, Apostolakis J, Arce P, Asai M, Aso T, et al. Recent developments in Geant4. Nucl Instrum Methods Phys Res A 2016; 835:186–225.
31. Francis Z, El Bitar Z, Incerti S, Bernal MA, Karamitros M, Tran HN. Calculation of lineal energies for water and DNA bases using the Rudd model cross sections integrated within the Geant4-DNA processes. J Appl Phys 2017; 122:14701.
32. Francis Z, Seif E, Incerti S, Champion C, Karamitros M, Bernal MA, et al. Carbon ion fragmentation effects on the nanometric level behind the Bragg peak depth. Phys Med Biol 2014; 59:7691–702.
33. Feng G, Liu L, Cui W, Wang F. Electron beam irradiation on novel coronavirus (COVID-19): A Monte–Carlo simulation. Chinese Phys B 2020; 29:048703.
34. GenBank: MN908947.3. Severe acute respiratory syndrome coronavirus 2 isolate Wuhan-Hu-1, complete genome. Bethesda, MD: National Center for Biotechnology Information. (https://bit.ly/37hMvFT)
35. Villagomez-Bernabe B, Chan SW, Coulter JA, Roseman A, Currell F. Fast ion beam inactivation of viruses, where radiation track structure meets RNA structural biology. bioRxiv 2020:2020.08.24.265553.
36. Francis Z, Villagrasa C, Clairand I. Simulation of DNA damage

Downloaded From: https://bioone.org/journals/Radiation-Research on 28 Mar 2024
Terms of Use: https://bioone.org/terms-of-use

clustering after proton irradiation using an adapted DBSCAN algorithm. Comput Methods Programs Biomed 2011; 101:265–70.

37. Friedland W, Jacob P, Bernhardt P, Paretzke HG, Dingfelder M. Simulation of DNA damage after proton irradiation. Radiat Res 2003; 159:401–10.

38. Martin F, Burrow PD, Cai Z, Cloutier P, Hunting D, Sanche L. DNA strand breaks induced by 0–4 eV electrons: The role of shape resonances. Phys Rev Lett 2004; 93:68101.

39. Brun E, Cloutier P, Sicard-Roselli C, Fromm M, Sanche L. Damage induced to DNA by low-energy (0–30 eV) electrons under vacuum and atmospheric conditions. J Phys Chem B 2009; 113:10008–13.

40. Boudaiffa B, Cloutier P, Hunting D, Huels MA, Sanche L. Resonant formation of DNA strand breaks by low-energy (3 to 20 eV) electrons. Science 2000; 287:1658–60.

41. Ebel K, Bald I. Length and energy dependence of low-energy electron-induced strand breaks in poly(A) DNA. Int J Mol Sci 2019; 21:111.

42. Agostinelli S, Allison J, Amako K, Apostolakis J, Araujo H, Arce P, et al. Geant4–a simulation toolkit. Nucl Instrum Methods Phys Res A 2003; 506:250–303.

43. Allison J, Amako K, Apostolakis J, Araujo H, Dubois PA, Asai M, et al. Geant4 developments and applications. IEEE Trans Nucl Sci 2006; 53:270–8.

44. Cascella M, Rajnik M, Cuomo A, Dulebohn SC, Napoli R Di. Features, evaluation and treatment coronavirus (COVID-19). In: StatPearls. Treasure Island, FL: StatPearls Publishing; 2020. (https://bit.ly/3aa7z31)

45. Guy JS, Breslin JJ, Breuhaus B, Vivrette S, Smith LG. Characterization of a coronavirus isolated from a diarrheic foal. J Clin Microbiol 2000; 38:4523–6.

46. Kim J-M, Chung Y-S, Jo HJ, Lee N-J, Kim MS, Woo SH, et al. Identification of coronavirus isolated from a patient in Korea with COVID-19. Osong Public Heal Res Perspect 2020; 11:3–7.

47. Shereen MA, Khan S, Kazmi A, Bashir N, Siddique R. COVID-19 infection: Origin, transmission, and characteristics of human coronaviruses. J Adv Res 2020; 24:91–8.

48. Liu J, Sun Y, Qi J, Chu F, Wu H, Gao F, et al. The membrane protein of severe acute respiratory syndrome coronavirus acts as a dominant immunogen revealed by a clustering region of novel functionally and structurally defined cytotoxic T-lymphocyte epitopes. J Infect Dis 2010; 202:1171–80.

49. Wang Q, Zhang Y, Wu L, Niu S, Song C, Zhang Z, et al. Structural and functional basis of SARS-CoV-2 entry by using human ACE2. Cell 2020; 181:894–904.e9.

50. Durante M, Cucinotta FA. Physical basis of radiation protection in space travel. Rev Mod Phys 2011; 83:1245–81.

51. Patera V, Prezado Y, Azaiez F, Battistoni G, Bettoni D, Brandenburg S, et al. Biomedical research programs at present and future high-energy particle accelerators. Front Phys 2020; 8:00380.

52. Lancker M, Bastiaansen L. Electron-beam sterilization. Trends and developments. Med Device Technol 2000; 11:18–21.

53. Fertey J, Bayer L, Grunwald T, Pohl A, Beckmann J, Gotzmann G, et al. Pathogens inactivated by low-energy-electron irradiation maintain antigenic properties and induce protective immune responses. Viruses 2016; 8:319.

54. Sanche L. Low energy electron-driven damage in biomolecules. Eur Phys J D 2005; 35:367–90.

55. Abdoul-Carime H, Sanche L. Alteration of protein constituents induced by low-energy (<35 eV) Electrons: II. Dissociative electron attachment to amino acids containing cyclic groups. Radiat Res 2003; 160:86–94.

56. Fluke DJ, Brustad T, Birge AC. Inactivation of dry T-1 bacteriophage by helium ions, carbon ions, and oxygen ions: Comparison of effect for tracks of various ion density. Radiat Res 1960; 13:788.

57. Schambra PE, Hutchinson F. The action of fast heavy ions on biological material: II. Effects on T1 and PHI-X-174 bacteriophage and double-strand and single-strand DNA. Radiat Res 1964; 23:514.

58. Smolko EE, Lombardo JH. Virus inactivation studies using ion beams, electron and gamma irradiation. Nucl Instrum Methods Phys Res B 2005; 236:249–53.

59. Waelzlein C, Kraemer M, Scifoni E, Durante M. Advancing the modeling in particle therapy: From track structure to treatment planning. Appl Radiat Isot 2014; 83:171–6.

60. David SC, Lau J, Singleton EV, Babb R, Davies J, Hirst TR, et al. The effect of gamma-irradiation conditions on the immunogenicity of whole-inactivated influenza A virus vaccine. Vaccine 2017; 35:1071–9.

61. Durante M, Indelicato P, Jonson B, Koch V, Langanke K, Meissner U-G, et al. All the fun of the FAIR: fundamental physics at the facility for antiproton and ion research. Phys Scr 2019; 94:033001.

62. Durante M, Golubev A, Park W-Y, Trautmann C. Applied nuclear physics at the new high-energy particle accelerator facilities. Phys Rep 2019; 800:1–37.

63. Fertey J, Thoma M, Beckmann J, Bayer L, Finkensieper J, Reisshauer S, et al. Automated application of low energy electron irradiation enables inactivation of pathogen- and cell-containing liquids in biomedical research and production facilities. Sci Rep 2020; 10:12786.

Downloaded From: https://bioone.org/journals/Radiation-Research on 28 Mar 2024
Terms of Use: https://bioone.org/terms-of-use